Report of Investigation 2024-8

LANDSLIDE HAZARD SUSCEPTIBILITY MAPPING IN HAINES, ALASKA

Jillian A. Nicolazzo and Martin C. Larsen

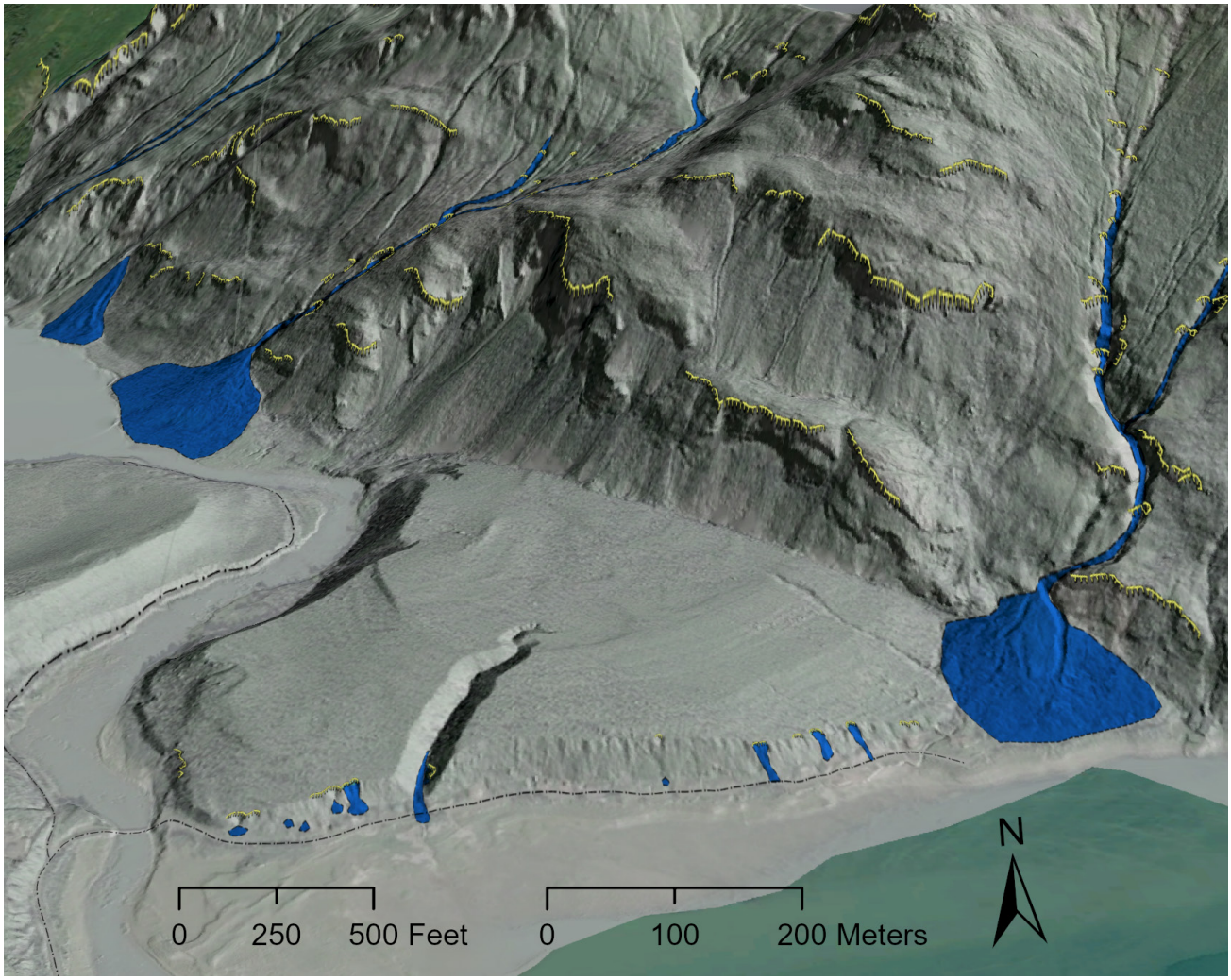

A partially transparent digital terrain model-derived hillshade raster over Esri's aerial image basemap, which shows a portion of the landslide inventory along Lutak Spur Road in Haines, Alaska.

Published by
STATE OF ALASKA
DEPARTMENT OF NATURAL RESOURCES
DIVISION OF GEOLOGICAL & GEOPHYSICAL SURVEYS
2025

LANDSLIDE HAZARD SUSCEPTIBILITY MAPPING IN HAINES, ALASKA

Jillian A. Nicolazzo and Martin C. Larsen

Report of Investigation 2024-8

State of Alaska
Department of Natural Resources
Division of Geological & Geophysical Surveys

STATE OF ALASKA
Mike Dunleavy, Governor

DEPARTMENT OF NATURAL RESOURCES
John Boyle, Commissioner

DIVISION OF GEOLOGICAL & GEOPHYSICAL SURVEYS
Melanie Werdon, State Geologist and Director

Publications produced by the Division of Geological & Geophysical Surveys (DGGS) are available for free download from the DGGS website (dggs.alaska.gov). Publications on hard-copy or digital media can be examined or purchased in the Fairbanks office:

Alaska Division of Geological & Geophysical Surveys
3354 College Rd., Fairbanks, Alaska 99709-3707
Phone: (907) 451-5010 Fax (907) 451-5050
dggspubs@alaska.gov | dggs.alaska.gov

DGGS publications are also available at:
Alaska State Library,
Historical Collections & Talking Book Center
395 Whittier Street
Juneau, Alaska 99811

Alaska Resource Library and Information Services (ARLIS)
3150 C Street, Suite 100
Anchorage, Alaska 99503

Suggested citation:
Nicolazzo, J.A., and Larsen, M.C., 2025, Landslide hazard susceptibility mapping in Haines, Alaska: Alaska Division of Geological & Geophysical Surveys Report of Investigation 2024-8, 16 p., 3 sheets. https://doi.org/10.14509/31309

Contents

Figures

Tables

Map Sheets

LANDSLIDE HAZARD SUSCEPTIBILITY MAPPING IN HAINES, ALASKA

Jillian A. Nicolazzo[1] and Martin C. Larsen[1]

Abstract

The deadly Beach Road landslide that occurred on December 2, 2020, in Haines, Alaska, highlights the significant safety and financial risks posed by slope failures to people and infrastructure. To better inform the Haines Borough of their potential landslide hazards and increase the city's hazard resiliency, the Alaska Division of Geological & Geophysical Surveys (DGGS) developed maps of historical and prehistorical slope failures, shallow landslide susceptibility, and modeled debris flow runouts.

The historical landslide inventory map integrates previously mapped landslides with newly mapped slope failures that we identified using high-resolution light detection and ranging (lidar) datasets and available aerial imagery. The shallow landslide susceptibility map is based on factor of safety calculations incorporating surficial mapping with soil engineering properties. The debris flow susceptibility map shows modeled inundation areas based on physical characteristics of the landscape that are derived from digital elevation models. The results of these analyses provide important information about the overall hazard in the region and can help guide future land-use planning and development. The results do not predict slope failures and do not replace detailed, site-specific investigations that should be conducted prior to development in susceptible areas. The datasets and maps are not regulatory and are not suitable for legal, engineering, or surveying purposes.

INTRODUCTION

An atmospheric river hit Southeast Alaska the first week of December 2020, which produced heavy rain in the Haines area. The rain fell on an existing snowpack on top of frozen and water-saturated soils, which caused flooding, road washouts, and numerous landslides. The landslide on Beach Road was widely publicized because it caused two fatalities. Dozens of landslides, debris flows, and flooding in other areas of town and across the Haines Borough also closed roads, impacted homes, and led to emergency evacuations. In total, eight homes were destroyed, and at least 21 were temporarily inaccessible. There was widespread and long-lasting disruption of daily life.

The Haines area has a long history of devastating landslides. In the 1880s, a landslide destroyed a village on the east bank of Chilkoot Lake, and many lives were lost (LeMay Engineering & Consulting, Inc., 2022). Oral history indicates this was not the first landslide of its type in this area. Heavy snow and rain in January of 1890 triggered a snow avalanche/landslide that destroyed buildings at the Pyramid Harbor Cannery (LeMay Engineering & Consulting, Inc., 2022). In 1914, a debris flow lasted for several days in Klukwan, a village approximately 37 km (23 mi) north of Haines (LeMay Engineering & Consulting, Inc., 2022). In 2011, a ground slump developed above Lutak Road and Oceanview Drive in Haines that fractured the road and disrupted plans for developing the neighborhood (Sheinberg Associates, 2012). Debris flows intermittently cover portions of the Haines Highway between about milepost 12

[1]Alaska Division of Geological & Geophysical Surveys, 3354 College Rd., Fairbanks, Alaska 99709-3707.

and 23, sometimes closing the road for days and costing the state hundreds of thousands of dollars annually (Alaska Department of Transportation & Public Facilities [DOT&PF], 2022).

The Haines Borough is currently updating its Hazard Mitigation Plan. The draft Plan states that the probability of ground failure in the Haines area is highly likely, equating to an event having a "one in one year's chance to occur" (LeMay Engineering & Consulting, Inc. 2022). To support Haines in becoming more resilient to potential hazards and to assist in the development of the Haines multi-hazard RiskMAP, the Alaska Division of Geological & Geophysical Surveys (DGGS) received funding from the Federal Emergency Management Agency (FEMA) Cooperating Technical Partners (CTP) Program to create an inventory database and map of historical landslides in addition to creating maps of landslide susceptibility for a selected area of interest (AOI) in the Haines Borough (fig. 1). The Haines Borough Assembly voted unanimously on February 9, 2021, in support of this project.

This report describes the datasets and methods used in this study and discusses the mapping and modeling results. Three map sheets accompany this report:

- Map Sheet 1: Landslide Inventory
- Map Sheet 2: Shallow Landslide Susceptibility
- Map Sheet 3: Channelized Debris Flow Susceptibility

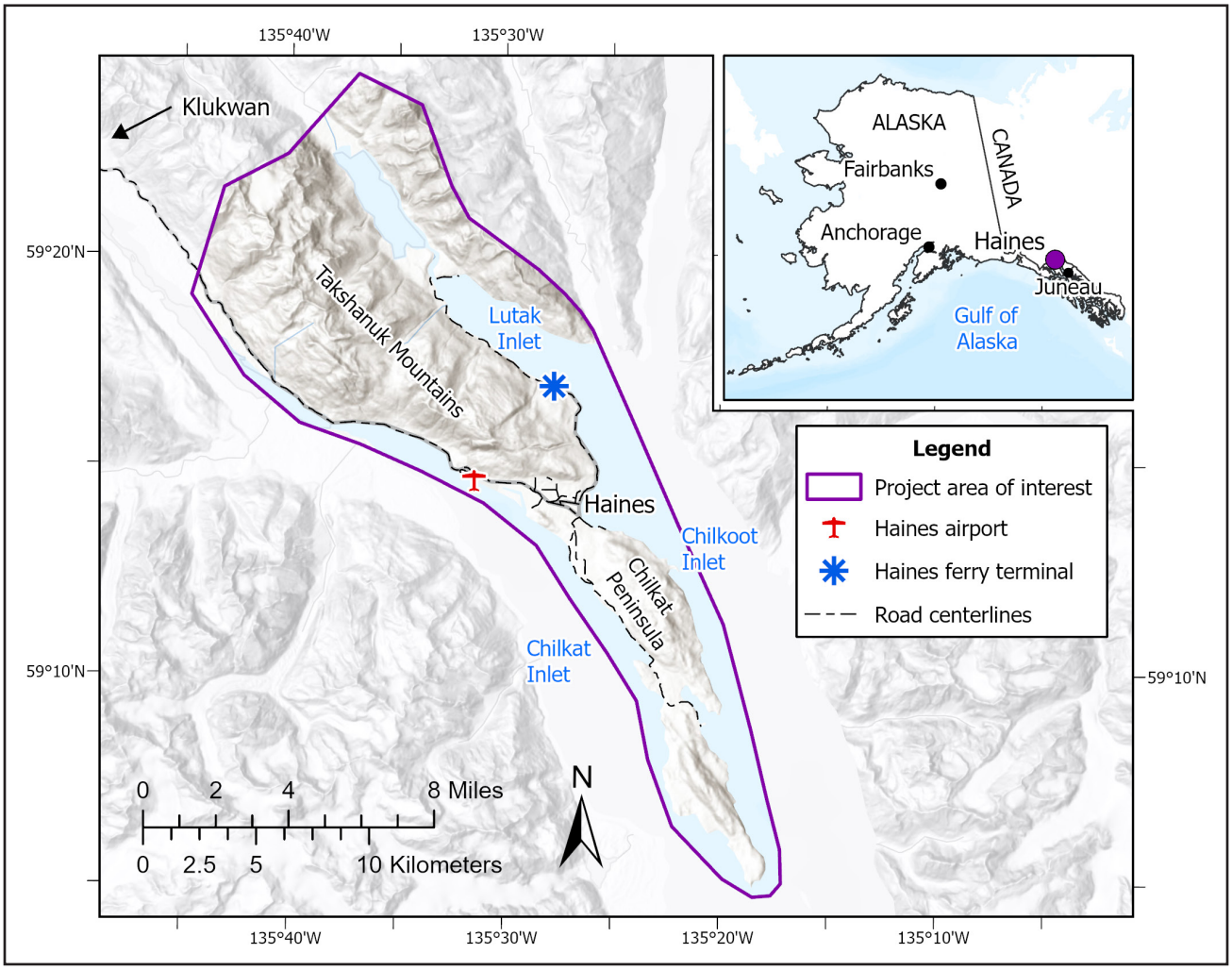

Figure 1. Project area of interest and major infrastructure displayed over Esri's World Terrain basemap.

EXISTING INFORMATION

Only one previously published geologic map (March, 1982) included landslide deposits in the Haines region. However, recent U.S. Geological Survey (USGS) STATEMAP-funded geologic mapping completed by DGGS identified additional landslides in the Haines area (Larsen, 2024). We included those landslides in this project's database and used STATEMAP project-identified surficial deposits as inputs for shallow landslide susceptibility modeling. In addition to this new mapping, there are numerous news articles, at least two published reports (Darrow and others, 2022; Landslide Technology, 2022), and a master's thesis (Nelson, 2023) that investigate the Beach Road landslide and debris flows, which were triggered by the storms in early December 2020.

Two light detection and ranging (lidar) datasets were previously collected for other projects in the Haines area that overlap this project's AOI. Quantum Spatial collected one dataset in May 2014 (~1-m [3-ft] resolution) that was centered primarily on the city of Haines (Quantum Spatial, 2014; fig. 2). In December 2020, DGGS collected lidar as part of emergency operations following the landslide event. The collection covered areas over the city of Haines, south along Mud Bay Road,

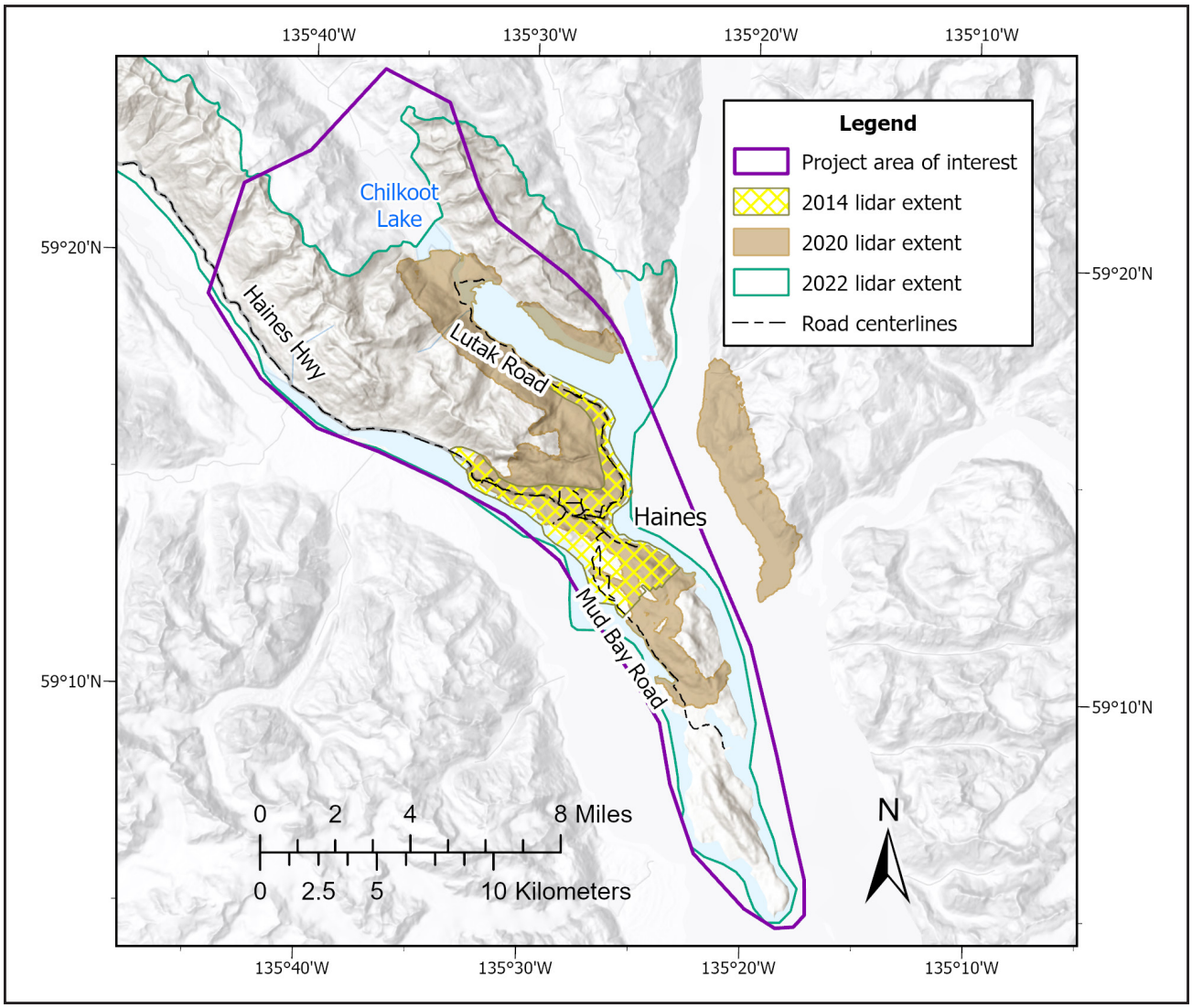

Figure 2. Extents of existing lidar datasets displayed over Esri's World Terrain basemap of the area of interest.

north along Lutak Road, and on the opposite side of Lutak Inlet with a 1-m (~3-ft) resolution (Daanen and others, 2021; fig. 2). Additionally, during 2021 and 2022, DGGS collected a new lidar dataset for this project, which covered a much larger area with a 50-cm (~1.5 ft) resolution (Zechmann and others, 2024; fig. 2). This project used digital terrain models (DTMs) generated from each of these lidar datasets. For the area around Chilkoot Lake where lidar was not collected, we downloaded data from ArcticDEM (Porter and others, 2022). The ArcticDEM is a composite of numerous digital elevation models (DEMs) sourced from satellite imagery collected over several years. It has 2-m (~6-ft) resolution and contains more elevation spikes, pits, and holes of missing data than our datasets; therefore, all results from the ArcticDEM dataset have lower confidence.

METHODS

The following sections describe the methods used to create each of the map sheets associated with this report: generating the inventory, shallow-landslide susceptibility mapping, and channelized debris flow susceptibility mapping. In general, we followed protocols developed by the Oregon Department of Geology and Mineral Industries (DOGAMI) and the Washington Department of Natural Resources (Burns and Madin, 2009; Burns and others, 2012; Burns and others, 2022; Slaughter and others, 2017).

Landslide Inventory Geodatabase and Map

In this section we use the word "landslide" generically to include all types of ground failure that we identified in the area, such as landslides, debris flows, rockfall, and creep. To generate the inventory, we followed landslide inventory mapping protocols described in Burns and Madin (2009) and Slaughter and others (2017).

We created three feature classes for this inventory using Esri's ArcGIS Pro, version 3.2: deposit polygons, flank polygons, and scarp polylines. The "ideal" landslide would have a mapped head scarp, possible internal scarps, flanks, and a deposit, but we rarely identified all these features. We could generally trace the scar from a paleo-landslide, but the head scarp, flank, and displaced material have often since eroded away; therefore, we included the extents of landslide scars in the deposit polygon. Mass movements in the Haines area are dominated by debris flows. Debris flows are confined to drainage channels and generally do not originate at a scarp, so these deposit polygons do not have associated scarps or flanks. We observed rockfall deposits at several road cuts; these might have an associated scarp polyline but no flank polygon. Erosional deposits such as colluvium and talus were not classified as landslides and do not have flank or deposit polygons, but we mapped scarp polylines for them because the bedrock is known to fail in these areas and could pose a hazard.

We created hillshade and slope rasters derived from lidar DTMs and used them to identify landslide and debris flow deposits within the project AOI. We identified the 2020 Beach Road landslide in the post-event DTM-derived rasters and used its geomorphological features as a calibration to identify other landslides. We also identified uplifted beach deposits in the rasters, and closely examined areas where these parallel lines were interrupted. We reviewed elevation differences between overlapping DTMs collected in different years to determine if the change was the result of slope instabilities (e.g., scour and deposition) or human activities (e.g., construction and material site mining), and then identified landslide scarps, flanks, and deposits throughout the AOI. Aerial imagery from multiple sources, including DGGS's 50-cm Maxar, Esri Wayback, and Google Earth, were used to supplement the DTMs.

Darrow and others (2022) identified numerous landslide scarps and several deposits on the Chilkat Peninsula, and Nelson (2023) identified more than 100 landslide scarps and dozens of deposits along Lutak Road while researching the 2020 storm event. We combined this data with landslides identified by DGGS geologists into a

single geodatabase with associated attribute data. The resultant inventory map is shown on map sheet 1. Each of the mapped landslides may represent a single occurrence or multiple reoccurring events.

Shallow-Landslide Susceptibility Mapping

In this section, we use the word "landslide" to refer to mass movements that have a distinct zone of weakness separating the slide materials from more stable underlying materials and to include both translational and rotational landslides. It does not include debris flows, which are discussed in the next section, nor seismically induced movements that require site-specific information and are outside the scope of this project. The susceptibility map does not include ground failures caused by seismic shaking such as liquefaction or lateral spread.

Following the methodology of Burns and others (2012), we developed a map showing slopes susceptible to shallow landslides. Shallow landslides occur in surficial soils, to a maximum depth of about 4.5 m (15 ft) (Burns and others, 2012). This method combines areas of mapped shallow landslides with a calculated factor of safety (FOS). The result is a map that displays susceptibility as high, moderate, or low zones (map sheet 2).

Factor of Safety

The FOS is the relationship between driving forces acting to move material downslope (e.g., gravity) and forces acting to resist downslope movement (e.g., soil cohesion; Burns and others, 2012; eq. 1). Slopes with an FOS greater than 1.0 are theoretically stable (the shear resistance is greater than the shear stress), and those with an FOS less than 1.0 are theoretically unstable (the stress is greater than the resistance). Since soil and rock composition and their geotechnical properties vary across geologic units, a conservative approach is appropriate, and an FOS less than 1.50 is generally considered to be unstable (Burns and others, 2012). For this project, FOS values less than 1.25 are classified as "highly" susceptible to failure, values from 1.25 to less than 1.50 are "moderately" susceptible to failure, and values equal to 1.50 or greater have low to no susceptibility to failure.

Equation 1.

$$FOS = \frac{c'}{\gamma\, t \sin\alpha} + \frac{\tan\phi'}{\tan\alpha} - \frac{m\,\gamma_w \tan\phi'}{\gamma \tan\alpha}$$

Where:

c' = effective cohesion

ϕ' = effective angle of internal friction

γ = saturated soil density (unit weight)

γ_w = groundwater density (unit weight)

t = depth to failure surface

m = groundwater depth ratio

α = slope angle

We relied on geologic mapping by Larsen (2024) to determine soil and rock units in the project area. Where available, published soil properties were used in the calculations (Lemke and Yehle, 1972; March, 1987; Landslide Technology, 2022; Nelson, 2023; Nicolazzo and others, 2024), and elsewhere they were estimated based on information from Filz (1982) and Geotech data (2023). Due to uncertainties and variations within a soil unit, we used conservative values (table 1).

Tchakalova and Ivanov (2022) provided equations to correlate the plasticity index of a soil to its effective cohesion. Plasticity index is obtained from Atterberg limits tests, and both Nicolazzo and others (2024) and Nelson (2023) provide Haines-specific soil properties that include Atterberg limits. Because the FOS equation is highly sensitive to cohesion, the more conservative approach was to assume there is very low or no cohesion where this value is unknown. We assumed the depth of failure was equal to the depth of a known failure plane or to bedrock, and to a maximum of 4.57 m (15 ft) (Burns and others, 2012). Where failure depth was unknown, we used a value of 4.57 m (15 ft). Based on the high average annual rainfall, the presence of several drainages, and the knowledge that landslides are more likely to occur after heavy rainfall when soils are saturated, we assigned a value of 1.0

Table 1. Factor of safety input parameters. See equation 1 for explanation of variables.

Soil Unit	Effective Angle of Internal Friction ϕ'	Effective Cohesion c'		Saturated Unit Weight of Soil γ		Depth of Failure		Groundwater Depth Ratio
	degrees	lb/ft^2	kPa	lb/ft^3	kN/m^3	ft	m	
Alluvial fan	27	50.0	2.4	105.0	16.5	15.0	4.6	1.0
Artificial fill	35	20.0	1.0	125.0	19.6	4.0	1.2	1.0
Bedrock, all types	45	460.0	22.0	180.0	28.3	3.0	0.9	1.0
Colluvium	22	50.0	2.4	102.0	16.0	5.0	1.5	1.0
Colluvium-alluvium	27	0.0	0.0	107.0	16.8	5.0	1.5	1.0
Delta	27	50.0	2.4	120.0	18.9	15.0	4.6	1.0
Elevated beach	34	0.0	0.0	125.0	19.6	15.0	4.6	1.0
Elevated marine	38	240.0	11.5	140.0	22.0	15.0	4.6	1.0
Elevated marine (younger)	38	240.0	11.5	140.0	22.0	15.0	4.6	1.0
Floodplain–active	24	0.0	0.0	100.0	15.7	15.0	4.6	1.0
Floodplain–inactive	27	0.0	0.0	120.0	18.9	15.0	4.6	1.0
Glacial outwash	30	100.0	4.8	118.0	18.5	15.0	4.6	1.0
Glacial outwash fan	30	100.0	4.8	118.0	18.5	15.0	4.6	1.0
Glacial till	42	300.0	14.4	145.0	22.8	15.0	4.6	1.0
Glacial-lacustrine	24	200.0	9.6	100.0	15.7	15.0	4.6	1.0
Landslide	28	0.0	0.0	110.0	17.3	15.0	4.6	1.0
Modern beach	34	0.0	0.0	125.0	19.6	15.0	4.6	1.0
Rock glacier	30	0.0	0.0	110.0	17.3	15.0	4.6	1.0
Talus	40	0.0	0.0	130.0	20.4	15.0	4.6	1.0

to the groundwater depth ratio for all soils, which implies a fully saturated condition.

We calculated the FOS for each soil type for the full range of possible slope angles from 1.0 to 90.0 degrees, in 0.5-degree increments, noting slope angles corresponding to an FOS of 1.25 and 1.50 for each soil type (table 2). In ArcGIS Pro, we used these threshold values to select areas with steeper slopes which we then reclassified to represent areas of high, moderate, and low susceptibility, and mosaicked them into a single raster. For example, areas mapped as alluvial fans are highly susceptible to failure when they are steeper than 11 degrees, are moderately susceptible between about 9.5 and 11 degrees, and have no or low susceptibility at slopes shallower than 9.5 degrees (table 2).

Buffers and Smoothing

We noted that numerous small, low-relief features such as ditches, retaining walls, road cuts, and house walls appear to have moderate or high susceptibility due to their steep elevation change in the high-resolution slope raster; however, these man-made features do not pose a significant hazard and their inclusion is misleading. To address this,

Table 2. Critical slope values per soil unit designating sloping areas moderately (FOS <1.50) and highly (FOS <1.25) susceptible to failure.

Soil Unit	Slope Angle Threshold for FOS <1.50	Slope Angle Threshold for FOS <1.25
	degrees	degrees
Alluvial fan	9.5	11.0
Artificial fill	15.0	17.5
Bedrock, all types	55.0	65.0
Colluvium	10.0	12.0
Colluvium-alluvium	8.5	10.0
Delta deposit	10.5	12.5
Elevated beach	13.0	15.5
Elevated marine deposit	20.5	24.5
Elevated marine deposit (younger)	20.5	24.5
Floodplain–active	6.5	8.0
Floodplain–inactive	9.5	11.5
Glacial outwash	12.5	15.0
Glacial outwash fan	12.5	15.0
Glacial till	24.0	28.5
Glacial-lacustrine	11.5	14.0
Landslide	9.0	10.5
Modern beach deposit	13.0	15.5
Rock glacier	9.5	11.5
Talus	16.5	19.5

we used the ArcGIS Pro Focal Statistics tool with a 3-m (9.8 ft) square neighborhood and 5-m (16.4 ft) vertical height to remove these structures from the raster. We ran several iterations of the tool and found that we could not remove all the structures without also removing areas of soil and bedrock that were correctly classified; therefore, we chose a combination that removed some of the man-made structures without compromising the accuracy of the analyses. This smoothing process also reduced the number of small, isolated susceptibility "islands" within a larger area of consistent susceptibility (e.g., a single cell or a few cells of low susceptibility within a high susceptibility rock cliff face).

Landslides tend to have a steep head scarp that may fail retrogressively, meaning a new landslide may form above the head scarp due to the removal of resisting material directly below and adjacent to the head scarp; therefore, flat areas near a head scarp may have a higher risk of failure than the FOS calculations indicate. To account for this increased risk, Burns and others (2012) recommend adding a buffer equal to 2 horizontal to 1 vertical (2H:1V) around head scarps. Due to the large number of scarps identified in this project, we generally did not differentiate head scarps from internal scarps or attempt to measure scarp heights. For this project, we applied this 2H:1V buffer to all

scarps and assumed the vertical distance was equal to 4.57 m (15 ft), which is the maximum depth of failure for all soils (table 1). The horizontal buffer distance is equal to 2x this depth, or approximately 9.1 m (30 ft). All areas within these buffer zones were assigned a "high" susceptibility rating because of their proximity to a mapped scarp, regardless of their FOS calculation. By buffering all scarps, bedrock faces that produce talus or colluvium, which might otherwise have been excluded, show a "high" susceptibility to failure.

Because landslides that originate on a steep slope can extend back into a flatter area above the slope or may have a toe that extends over a flat area at the bottom, Burns and others (2012) also recommend applying a similar 2H:1V buffer to all areas with a calculated FOS less than or equal to 1.5. We applied the ArcGIS Pro Expand tool to the smoothed raster to create this buffer. Areas within the expansion were assigned a "moderate" susceptibility rating, effectively creating a halo of moderate susceptibility around areas of moderate or high susceptibility.

The resulting map (map sheet 2) is a composite of the extracted landslide inventory, factor of safety calculations, buffers, and surface smoothing.

Channelized Debris Flow Susceptibility Mapping

Debris flows are a form of mass movement characterized by a slurry of water, soils, rocks, trees, and other debris quickly moving downslope under the influence of gravity. They are often associated with large rain events and are among the most destructive and expensive geologic hazards that occur in Alaska (Division of Homeland Security & Emergency Management, 2023).

Burns and others (2022) describe a method to map slopes that are susceptible to channelized debris flows and include custom ArcGIS geoprocessing tools to simplify the process. This method models debris flow initiation potential, transport potential, and inundation (deposition) to produce a map that displays debris flow initiation and transport susceptibility in high, moderate, or low zones, and the inundation extent for each level of modeled event severity (map sheet 3).

Initiation

To verify that the protocol developed by Burns and others (2022) is applicable to Southeast Alaska, or to determine if the input values should be adjusted, we followed the methods described in Burns and others (2022). We did not identify enough translational or rotational landslides in the Haines area to use as a basis for this study, so we used the Tongass National Forest (TNF) landslide inventory compiled by the U.S. Forest Service (2022a; 2022b). We used elevation data from Wrangell (Zechmann and others, 2023) and Prince of Wales (National Oceanic and Atmospheric Administration Office for Coastal Management Partners, 2018, 2020) islands due to the large number of identified landslides and initiation points and the amount of high-resolution lidar data. We extracted slope and curvature information for the TNF landslide initiation points from the DTMs and compared the histograms to those of Burns and others (2022).

We found the average slope to be 37 and 39 degrees for Wrangell Island and Prince of Wales Island, respectively, with a standard deviation of about 9 degrees. This closely matches those of Burns and others (2022), which averaged 39 degrees with a standard deviation of 4.6 degrees. However, their curvature average was -1.0, whereas ours was nearly 0. A value of 0 implies planar ground, but we are most interested in areas where loose soil and water can accumulate (negative values). Because the TNF inventory was primarily created through review of aerial imagery rather than lidar data, the initiation points may not be precisely located. We determined it would be too time-prohibitive to review all the points and adjust them based on their locations in the DTMs, especially since they are not within this project's area of interest, so we retained Burns and others (2022) suggested value of -1.0.

The protocol developed by Burns and others (2022) uses a curvature-based method for identifying drainage channels. They used a concavity threshold of -2.0, but this output appeared to underrepresent the number of drainages in the Haines area; when the model was complete, the final inundation did not match observations during the 2020 storms. We tried various combinations and determined that a curvature threshold of -1.5 resulted in more channels and a better representation of the Haines area. When multiple iterations were run, the "minimum concavity size" and "contributing concave area" inputs did not appear to change the output significantly; we used values of 10 m^2 (107.6 ft^2) and 200 m^2 (2,152.8 ft^2), respectively, as suggested by the protocol (Burns and others, 2022). These same values were used again in the Laharz model, described in the Inundation/Deposition section of this report.

We assigned values of 1 to 4—corresponding to no, low, moderate, and high susceptibility, respectively—to a range of slope and curvature raster values. Slopes 55 degrees and greater were not included in the analysis since they are less likely to accumulate the colluvium (loose, unconsolidated sediment) necessary for channelized debris flow initiation (Burns and others, 2022). The curvature raster identifies topography that is concave or convex and indicates where water and colluvium might collect (in concavities, negative values) or be dispersed (from convexities, positive values). Debris flows tend to initiate in or near an existing drainage channel, so the distance to a channel was also included in the initiation potential (Burns and others, 2012; table 3).

The final initiation potential score is the sum of the slope, curvature, and distance values, culminating in a single value, which is then classified as high, moderate, low, or very low/no susceptibility (table 4).

Transport

Once a debris flow begins to travel down a channel, certain conditions must exist for it to continue to flow. Burns and others (2022) use channel gradient and confinement as the two primary criteria to define the transportation potential of a flowing channelized debris flow. Their tool divides the drainage network created in an earlier step (see

Table 3. Summary of values for debris flow initiation potential.

Assigned Value	Category	Slope (degrees)	Curvature	Distance to drainage	
			0.0035 m (1/100 ft)	ft	m
4	High	35 to <55	≤ -0.4	≤100	≤30.5
3	Moderate	25 to ≤35	-0.4 to ≤0.3	100 to ≤200	30.5 to ≤61
2	Low	15 to ≤25	0.3 to ≤1.1	200 to ≤300	61 to ≤91.4
1	Very low to none	≤15	>1.1	>300	>91.4

Table 4. Final debris flow initiation susceptibility scores.

Score (Slope + Curvature + Distance)	Susceptibility Class
11 and 12	High
8 to 10	Moderate
5 to 7	Low
4 or less	Very low to none

Initiation) into 30.5-m (100-ft) segments, which are used as the flow paths for transportation potential.

Channel gradient is the downhill slope of the channel, defined by the number of meters (feet) the channel drops per kilometer (mile) along its length. Steeper channel gradients are more likely to transport debris flows than shallower gradients, and debris is more likely to deposit where the gradient becomes shallower (Burns and others, 2022).

Channel confinement is defined as the ability of a channel to move laterally. It is the relationship between the channel width and the surrounding landscape, floodplain, or valley. The tool created by Burns and others (2022) transects the channel segments perpendicularly at 8-m (25-ft) intervals that extend 30.5 m (100 ft) to either side of the channel line, creating five transect lines per segment. Points are placed at 3-m (9-ft) intervals along the transect lines, and the elevation at each point is extracted from the DTM. The difference between the highest and lowest elevation values for each transect line is calculated, and the average of the differences for the five transect lines for each channel segment is calculated and assigned to that channel segment. This value defines the amount of confinement for that segment; a difference of 3 m (10 ft) along the 30.5-m (100-ft) segment indicates low confinement (i.e., the channel can more easily shift side to side), whereas a difference of 23 m (75 ft) along the 30.5-m (100-ft) segment indicates high confinement (i.e., the channel cannot easily shift laterally).

We used the value ranges suggested by Burns and others (2022) for this project (table 5). The final channel transport susceptibility score is the sum of the confinement value of each segment and the channel gradient value (table 6).

Watershed

A watershed is the upslope area that contributes flow to a common outlet. The tool created by Burns and others (2022) generates watersheds using standard hydrography tools in ArcGIS Pro and applies user-defined pour points (outlets) and the transport channels created in an earlier step (see

Table 5. Summary of values for channel transport potential (Burns and others, 2022).

Assigned Value	Category	Confinement		Gradient
		Vertical Feet Per 100-Foot Increment	Vertical Meters Per 30.5-Meter Increment	Degrees
4	High	40 and greater	12 and greater	15 and greater
3	Moderate	20 to <40	6 to <12	7.5 to <15
2	Low	10 to <20	3 to <6	5 to <7.5
1	Very low to none	≤10	≤3	≤5

Table 6. Final channel transport susceptibility scores (Burns and others, 2022).

Score (Confinement + Gradient)	Susceptibility Class
8	High
6 and 7	Moderate
4 and 5	Low
Less than 4	Very low to none

Transport). Watershed susceptibility is a combination of initiation and transportation potentials and is based on the estimated number of initiation sites per area and the percent of transport channels with high or moderate susceptibility (Burns and others, 2022; table 7). Using ArcGIS, initiation and transport susceptibility scores are joined to each watershed polygon and summed to create a final watershed susceptibility score (Burns and others, 2022; table 8). This score does not take into account how long it might take for debris to accumulate after an event or how much water is flowing; it assumes a sufficient volume of material that can be transported is always available and that there is always water flowing fast enough to transport it.

Inundation/Deposition

We used the Laharz model to simulate debris flow inundation/deposition. Laharz is a computer model developed for the USGS that simulates the behavior of volcanic mudflows, known as lahars, and was modified to include channelized debris flows (Schilling, 1998). Burns and others (2022) extended the Laharz model to include the ability for volumes to expand as they flow down channel.

Burns and others (2022) recommend modeling debris flows for three hazard scenarios: typical, intermediate, and extreme. The "typical" scenario has a small to medium impact and a high relative reoccurrence interval; this event might occur every few years or decades. An "extreme" scenario has a large to extreme impact and a low relative reoccurrence interval; it might happen once per millennia or less frequently. Characteristics of an "intermediate" scenario fall between typical and extreme. Two input values are required for modeling each scenario: growth factor and maximum volume. Growth factor defines the erosion and entrainment of debris that add to the volume of a debris flow moving down the channel. The maximum volume limits how large the debris flow can grow. Input values for the typical scenario are selected and adjusted until the modeled inundation area overlaps and closely matches observed debris flows in the area. These values are then scaled-up to obtain

Table 7. Summary of values for watershed potential (Burns and others, 2022).

Assigned Value	Category	Number of Estimated Potential Initiation Sites per Watershed	Percent of High and Moderate Channels in Watershed
4	High	5 and greater	50 and greater
3	Moderate	1 to <5	25 to <50
2	Low	0.5 to <1	10 to <25
1	Very low to none	Less than 0.5	Less than 10

Table 8. Final watershed susceptibility score (Burns and others, 2022).

Score (initiation site + susceptible channels)	Susceptibility Class
8	High
6 and 7	Moderate
4 and 5	Low
Less than 4	Very low to none

corresponding values for the intermediate and extreme scenarios (Burns and others, 2022).

We found that the growth factor was the more significant variable in determining inundation/deposition; the maximum volume rarely limited the inundation output. We modeled the typical scenario with a growth factor of 0.10 m^3/m^3 (0.30 ft^3/ft^3) and a maximum volume of 100,000 m^3 (3,531,467 ft^3) and the extreme scenario with a growth factor of 1.0 m^3/m^3 (3.3 ft^3/ft^3) and a maximum volume of 250,000 m^3 (8,828,667 ft^3). We did not model the intermediate scenario because it did not add any significant value to the dataset.

We manually selected the locations where debris flows would begin to slow down and deposit material. We placed these "pour point" locations along the transport channels created in an earlier step (see Transport) based on a decrease in slope gradient and where the potential for upslope initiation and transport decreased to "low" or "very low to none." Because these modeled channels are DTM-based, they incorrectly followed roadside ditches in some places, which resulted in the deposition of material in unrealistic locations. In these cases, we adjusted the DTM by adding lower elevation polylines through the road embankment to simulate either flow through an existing culvert or overtopping of the road by debris.

We used Esri's Boundary Clean tool to smooth the final inundation rasters and then convert them to polygons to further smooth the edges and to remove unrealistic deposition spikes. Some polygons were then also adjusted to remove areas that were likely incorrectly classified due to interpolation errors in the production of the lidar-derived DTMs.

RESULTS AND DISCUSSION

Landslide Inventory and Database

Based primarily on interpretation of lidar-derived DTMs, we identified debris flow, landslide and rockfall deposits, and evidence of possible creep. We did not further classify these movements into sub-types, so all are considered "undifferentiated" in this context. The Beach Road landslide of 2020 has been more extensively studied and is identified separately on the inventory map (map sheet 1). We identified the following mass movements in the Haines area, and the following descriptions are summarized from Highland and Bobrowsky (2008).

Debris flow

The debris flow category presented here may include channelized debris flows, earthflows, mudflows, etc. This form of mass movement may include loose soils and debris mixed with water to form a slurry that quickly moves downslope. They are most likely to occur in steep channels and are often associated with large rain events. Faster-moving water carries larger particles, such as sands and gravels, while slow-moving water might only carry silt or smaller particles. High winds are sometimes associated with debris flows because they can cause tree throw that exposes soils. Vegetation helps stabilize soils, so the removal of vegetation (through tree throw, wildfires, or man-made clearing) may increase the likelihood or severity of debris flows by removing the soil's protective layer. We identified debris flow deposits at most drainage channels, although some of this transported material could be the result of alluvial processes.

Landslide

The landslide category presented here may include translational and rotational landslides, as well as areas where bedrock lineaments (e.g., small faults) have released and shifted. Translational landslides are downslope movements of a soil or rock mass that occur along a failure plane, contact between different materials, or other zone of shear strain. The mass may move out and down with little or no rotation. Rotational landslides occur along a curved rupture. The upper portion of the displaced material moves downward and tilts backwards toward the head scarp, while the toe may shift upward and form a bump. Both types can be triggered by a rise in groundwater due to rainfall, rapid snowmelt, flooding, and/or human influences

such as irrigation, leaking pipes, filling reservoirs, etc. We identified numerous small landslide scarps along riverbanks that we included in the inventory even though they may be due to riverine erosional processes rather than landslides.

Rockfall

The rockfall category presented here includes rockfall and rock topple, which are rock masses that detach and fall, roll, bounce, or rotate out and down. They are common on near-vertical slopes in both bedrock and along riverbanks and coastal areas. Although we only identified rockfall as occurring at road cuts in this inventory, there are colluvium and talus deposits below bedrock scarps that some might also include in this category.

Creep

Creep is the very slow downslope movement of sediment that generally only occurs during certain times of the year or under specific conditions. In Alaska, we see this most often at northern latitudes or at high alpine elevations where it occurs as solifluction due to recurrent freeze/thaw processes. Although Haines is generally not considered to be a permafrost environment, areas at higher elevations may be frozen all year. We identified two areas with characteristics similar to solifluction that were large enough to map. Both areas appear to have overflow water, rather than an incised channel, that slowly moves soils downslope toward a more established drainage.

Susceptibility Maps

In general, steeper slopes and those comprised of loose, non-cohesive soils are more susceptible to shallow landslides as compared to gentler slopes and those with dense or cohesive soils. Our conservative analysis suggests that slopes steeper than ~15 degrees should be considered susceptible to movement; however, several assumptions were made regarding soil engineering properties and depth of failure. Our analysis also assumes saturated soil conditions and did not consider slope stabilization from vegetation or human mitigation efforts. The landslide susceptibility map highlights areas that may be more susceptible to landslides and may warrant further investigation before development; it does not predict landslide probability or frequency (map sheet 2).

Most drainages in the Haines Borough have the potential to cause debris flows, with known impacts varying from the deposition of small sand piles that are confined to road ditches, to very large events that inundate roads and damage structures (map sheet 3). In our analysis, we assumed that a static volume of material was available, and we did not consider how long it might take for material to re-accumulate after an event. We did not consider the volume of flowing water, flow speed, or the effects of drought or sudden, intense rainfall. Large trees or other objects in a moving debris flow can change the runout path. Buildings and other structures in the runout path can also alter the direction of debris flow; we did not take these factors into consideration. As with the shallow landslide susceptibility map, the channelized debris flow map presents areas where debris flows might originate and where they might deposit; it does not predict their probability or frequency.

INTENDED USE AND LIMITATIONS

The intended use of these maps is to help identify the relative slope failure hazard in the Haines Borough, to provide a basis for regional planning and increased resiliency, and to help identify areas where more detailed landslide mapping is warranted. Limitations of the input data and modeling methods are such that the maps are not suitable to answer site-specific or legal questions. These maps should only be used for regional- or community-scale purposes and are not intended to be viewed at scales other than the published map scale (1:25,000). They are not suitable for land-use regulation, building-code development, or to answer legal questions.

The Haines Borough landslide inventory and susceptibility maps were developed using the best available data; however, some of the limitations include:

- Lidar provides a "snapshot" view of the landscape at the time of data collection; therefore, maps based on lidar data interpretation may become less accurate as new landslides or other changes to the landscape occur or new technology that would improve the data products becomes available.
- Lidar data interpretation may also change as new terrain feature interpretation techniques develop.
- While every reasonable effort was made to map all slope failures, given the limitations in lidar datasets, available imagery, field validation, and vegetation density, it is likely that some slope failures were missed, overlooked, or misinterpreted by the authors. As new information and improved technology become available, we expect that future mapping will identify additional events that our analysis missed with greater accuracy and confidence.
- The lidar-based DTM cannot distinguish elevation changes due to man-made structures (e.g., buildings and other structures) from natural elevation changes (e.g., landslide scour and deposition).
- Because it is not feasible to collect detailed site-specific information on every landslide, assumptions and estimations were made.
- The FOS calculations were done per soil unit and are strongly influenced by the accuracy and resolution of the input data for soil unit extents, material properties, depth to failure, depth to groundwater, and slope angle. Material properties were estimated based on soils data from several sources and are conservative estimates. Slope angle was derived from a 50-cm (~1.5-ft) DTM.
- FOS calculations were done per individual cell, without regard for the adjacent cells. We resampled slopes to 3-m (~10-ft) resolution and applied focal statistics to reduce the "noise" of processing interpolation and local overestimation in areas of steep slopes with low relief; however, some localized overestimations are still possible.
- Debris flow runout modeling is based on estimates of growth factor and volume. While these estimates are based on our best assessment of the data, differences in these estimates and actual debris flow runouts are possible.
- Interaction of debris flows with buildings and any changes to grade or other mitigation measures can change the direction of flow. Large trees in a debris flow can also affect its runout length and width and could not be accounted for in the modeling.
- This report and maps are non-regulatory.

CONCLUSION

DGGS completed this landslide hazard assessment for the Haines Borough by creating a map and database of historical and prehistorical slope failures, a map of shallow landslide susceptibility, and a map of simulated debris flow runouts for a portion of the Haines Borough. Data from these analyses are collectively intended to depict the overall hazard, the results of which provide important information that can help guide planning and future risk investigations. The maps are not intended to predict the probability or reoccurrence of slope failures, and site-specific, detailed investigations should be conducted prior to development in potentially hazard-prone areas. Results are for informational purposes and are not intended for legal, engineering, or surveying uses.

Care should be taken before development on and near existing landslide and debris flow deposits. Many of the drainages in Haines' steep catchments are conduits for debris and many have debris flow fans at their bases, indicating that debris flows have occurred there in the past. Most of these features were identified using remotely sensed data, with limited field verification. We recommend site-specific investigations by qualified engineers to evaluate risk in areas where future development intersects zones identified as having moderate or high susceptibility to slope failures.

ACKNOWLEDGMENTS

DGGS collected and processed lidar data and conducted landslide susceptibility mapping for this project using funds provided by the Federal Emergency Management Agency (FEMA) Cooperative Technical Partnership (CTP) Program grant number CTP EMS-2021-CA-00013-S01.

We thank our reviewers Katreen Wikstrom Jones (DGGS) and Jacqueline Foss (U.S. Forest Service) for their thoughtful comments that helped improve the quality of this product. We also appreciate DOT&PF engineer Travis Eckhoff, P.E., for his local knowledge that helped verify our models, and Dr. Margaret Darrow (University of Alaska Fairbanks) for her insight into the Beach Road landslide. We also acknowledge Victoria Nelson for her countless hours spent performing soil laboratory testing and mapping landslide scarps in support of this project while working on her master's thesis.

REFERENCES

Alaska Department of Transportation & Public Facilities, 2022, Geo. Event Tracker-download event data. akdot.maps.arcgis.com/sharing/rest/content/items/44a003d1b33945b0ba5284ca9abddd14/data

Burns, W.J., Franczyk, J.J., and Calhoun, N.C., 2022, Protocol for channelized debris flow susceptibility mapping: Oregon Department of Geology and Mineral Industries Special Paper 53, 89 p. pubs.oregon.gov/dogami/sp/SP-53/p-SP-53.htm

Burns, W.J., and Madin, I.P., 2009, Protocol for inventory mapping of landslide deposits from light detection and ranging (lidar) imagery: Oregon Department of Geology and Mineral Industries Special Paper 42, 30 p. www.oregongeology.org/pubs/sp/p-SP-42.htm

Burns, W.J., Madin, I.P., and Mickelson, K.A., 2012, Protocol for shallow landslide susceptibility mapping: Oregon Department of Geology and Mineral Industries Special Paper 45, 32 p. www.oregongeology.org/pubs/sp/p-SP-45.htm

Daanen, R.P., Herbst, A.M., Wikstrom Jones, Katreen, and Wolken, G.J., 2021, High-resolution lidar data for Haines, Southcentral Alaska, December 8-12, 2020: Alaska Division of Geological & Geophysical Surveys Raw Data File 2021-4, 8 p. https://doi.org/10.14509/30595

Darrow, M.M., Nelson, V.A., Grilliot, Michael, Wartman, Joseph, Jacobs, Aaron, Baichtal, J.F., Buxton, Cindy, 2022, Geomorphology and initiation mechanisms of the 2020 Haines, Alaska landslide: Landslides, v. 19, p. 2,177–2,188. doi.org/10.1007/s10346-022-01899-3

Division of Homeland Security and Emergency Management, 2023, State of Alaska state hazard mitigation plan, p. 465. ready.alaska.gov/Mitigation/SHMP

Filz, George, 1982, Engineering properties of southeast Alaskan forest soils. Oregon State University, M.S. thesis, 51 p. ir.library.oregonstate.edu/downloads/mw22v9355

Geotech data, 2023, Geotechnical Parameters. [accessed July 2024] www.geotechdata.info/parameter/

Highland, L.M., and Bobrowsky, Peter, 2008, The landslide handbook—A guide to understanding landslides: U.S. Geological Survey Circular 1325, 129 p. pubs.usgs.gov/circ/1325/

Landslide Technology, 2022, Updated Findings Report, Beach Road Landslide, Haines, Alaska, 141 p. www.hainesalaska.gov/media/33306

Larsen, M.C., ed., 2024, Geologic map and map unit description for Haines, Alaska: Alaska Division of Geological & Geophysical Surveys Preliminary Interpretive Report 2024-9. doi.org/10.14509/31417

LeMay Engineering & Consulting, Inc., 2022, Haines Borough Hazard Mitigation Plan Update, 216 p. www.hainesalaska.gov/media/58551

Lemke, R.W., and Yehle, L.A., 1972, Reconnaissance engineering geology of the Haines area, Alaska, with emphasis on evaluation of earthquake and other geologic hazards: U.S. Geological Survey Open-File Report 72-229, 109 p., 2 sheets, scale 1:24,000

March, G.D., 1982, Photointerpretive map of the surficial geology of the Skagway B-2 Quadrangle, Alaska: Alaska Division of Geological & Geophysical Surveys Alaska Open-File Report 161, 1 sheet, scale 1:63,360. doi.org/10.14509/96

———1987, Surficial geology and materials-resources maps of the Skagway A-2 Quadrangle, Alaska: Alaska Division of Geological & Geophysical Surveys Report of Investigation 87-6, 2 sheets, scale 1:63,360. doi.org/10.14509/2429

Nelson, V.A., 2023, An analysis of cataloged December 2020 landslides near Haines, Alaska: Fairbanks, Alaska, University of Alaska Fairbanks, M.S. thesis, 174 p. scholarworks.alaska.edu/handle/11122/13244

Nicolazzo, J.A., Darrow, M.M., and Walser, S.L., 2024, Soil index properties and radiocarbon ages of the Haines-Takshanuk Mountains-Chilkat Peninsula area STATEMAP project, Southeast Alaska: Alaska Division of Geological & Geophysical Surveys Raw Data File 2024-27, 24 p. doi.org/10.14509/31415

National Oceanic and Atmospheric Administration (NOAA) Office for Coastal Management Partners, 2018, 2017 USGS Lidar: Prince of Wales Island, AK, NOAA National Centers for Environmental Information. www.fisheries.noaa.gov/inport/item/58254

———2020, 2018 USGS Lidar: Prince of Wales Island - Phase 2, AK, NOAA National Centers for Environmental Information. www.fisheries.noaa.gov/inport/item/59311

Porter, Claire, Howat, Ian, Noh, Myoung-Jon, Husby, Erik, Khuvis, Samuel, Danish, Evan, Tomko, Karen, Gardiner, Judith, Negrete, Adelaide, Yadav, Bidhyananda, Klassen, James, Kelleher, Cole, Cloutier, Michael, Bakker, Jesse, Enos, Jeremy, Arnold, Galen, Bauer, Greg, and Morin, Paul, 2022, ArcticDEM–Strips, Version 4.1: University of Minnesota Polar Geospatial Center Harvard Dataverse. doi.org/10.7910/DVN/C98DVS

Quantum Spatial, 2014, Skagway, Haines, and Petersburg lidar Technical Data Report: Fairbanks, AK. elevation.alaska.gov/

Schilling, S.P., 1998, LAHARZ; GIS programs for automated mapping of lahar-inundation hazard zones: U.S. Geological Survey Open-File Report 98-638, 80 p. doi.org/10.3133/ofr98638

Sheinberg Associates, 2012, Haines Borough 2025 Comprehensive Plan. www.hainesalaska.gov/media/59571

Slaughter, S.L., Burns, W.J., Mickelson, K.A., Jacobacci, K.E., Biel, Alyssa, and Contreras, T.A., 2017, Protocol for landslide inventory mapping from lidar data in Washington State: Washington Geological Survey Bulletin 82, 27 p. www.dnr.wa.gov/Publications/ger_b82_landslide_inventory_mapping_protocol.zip

Tchakalova, Boriana, and Ivanov, Plamen, 2022. Correlation between effective cohesion and plasticity index of clay: Geologica Balcanica, v. 51, no. 3, p. 45–49. www.geologica-balcanica.eu/sites/default/files/articles/Tchakalova_Geol_Balc_51-3_2022_0.pdf

U.S. Forest Service, 2022a, Tongass landslide initiation: U.S. Department of Agriculture Forest Service. [accessed April 2024] gis.data.alaska.gov/datasets/72786660fa974cb68b390c1f41730d19/about

U.S. Forest Service, 2022b, Tongass National Forest: Tongass National Forest Landslide Areas: U.S. Department of Agriculture Forest Service. [accessed April 2024] data-usfs.hub.arcgis.com/datasets/112e05629a304613b4fda6057225d60d/about

Zechmann, J.M., Daanen, R.P., Wikstrom Jones, K.M., and Wolken, G.J., 2024, Lidar-derived elevation data for Haines, Southeast Alaska, collected October 2021 and October 2022: Alaska Division of Geological & Geophysical Surveys Raw Data File 2023-18, 16 p. doi.org/10.14509/31034

Zechmann, J.M., Wikstrom Jones, K.M., and Wolken, G.J., 2023, Lidar-derived elevation data for Wrangell Island, Southeast Alaska, collected July 2023: Alaska Division of Geological & Geophysical Surveys Raw Data File 2023-28, 14 p. doi.org/10.14509/31098